Mismatched front and back gratings for optimum light trapping in ultra-thin crystalline silicon solar cells

Citation: Hsu, Wei-Chun, Jonathan K. Tong, Matthew S. Branham, Yi Huang, Selçuk Yerci, Svetlana V. Boriskina, and Gang Chen. "Mismatched Front and Back Gratings for Optimum Light Trapping in Ultra-Thin Crystalline Silicon Solar Cells." Optics Communications 377 (October 2016): 52–58.

As Published: http://dx.doi.org/10.1016/j.optcom.2016.04.055

Publisher: Elsevier

Persistent URL: http://hdl.handle.net/1721.1/118632

Version: Final published version: final published article, as it appeared in a journal, conference proceedings, or other formally published context

Mismatched Front and Back Gratings for Optimum Light Trapping in Thin Crystalline Silicon Solar Cells

Wei-Chun Hsu,[1] Jonathan K. Tong,[1] Matthew S. Branham,[1] Yi Huang,[1] Selçuk Yerci,[1,2] Svetlana V. Boriskina, [1,a)] and Gang Chen[1,b)]

[1]*Department of Mechanical Engineering, Massachusetts Institute of Technology, Cambridge, Massachusetts 02139, USA*

[2]*Micro and Nanotechnology Programme, Electric and Electronics Engineering, and the Center for Solar Energy Research and Applications, Middle East Technical University, Ankara 06800, Turkey.*

ABSTRACT

The implementation of a front and back grating in thin photovoltaic cells is a promising approach towards improving light trapping. A simple design rule was developed using the least common multiple (LCM) of the front and back grating periods. From this design rule, several optimal period combinations can be found, providing greater design flexibility for absorbers of indirect band gap materials. Using numerical simulations, the photo-generated current (J_{ph}) for a 10-μm-thick crystalline silicon absorber was predicted to be as high as 38 mA/cm^2, which is 11.74% higher than that of a single front grating (J_{ph}=34 mA/cm^2).

KEYWORDS : Light trapping, double grating, crystalline silicon, solar cell, thin absorber

1. Introduction

Solar photovoltaics (PV) technology has advanced considerably in recent years with current state-of-the-art single junction PV cells exhibiting efficiencies approaching the Shockley-Queisser limit.[1] The need to reduce costs have spurred the development of thin-film PV devices. Conventional bulk crystalline silicon (c-Si) PV cells typically have device thicknesses of 140-180 μm and require a 300-μm-thick wafer to produce one cell due to kerf losses associated with Si boules dicing. Including kerf losses, raw material costs have been shown to contribute over 30% of total module cost in conventional PV cells.[2-4] To produce thin c-Si cells without excessive material waste, new manufacturing technologies have been recently developed including silicon epitaxial growth and direct wafering.[5-8] Despite the cost benefits, the combination of an indirect band gap and thinness of the absorber make thin c-Si cells a poor absorber of near-infrared light, leading to significant photocurrent losses. Therefore, light trapping is paramount for thin c-Si PV cells to approach the Shockley-Queisser limit.

In order to enhance light-trapping performance, a myriad of structures using surface plasmons,[9-11] photonic crystals,[12-14] or diffraction gratings[12-40] were proposed. In particular, diffraction gratings incorporated onto the front of PV cells have shown great potential by coupling incident light into guided modes in the thin film. Additionally, recent studies have shown that triangular, pyramidal, or conical gratings exhibit higher absorption due to the impedance match from air to silicon.[15-22,28,30,39] To improve light trapping even further, the inclusion of a back grating structure has been studied as a means to better scatter near-infrared light into guided resonances.[12-14,17,27-28,33] By combining a front and back grating, recent studies have demonstrated enhancement to light trapping that outperforms absorbers that are textured only on one side.[27-39] Further improvements for these double grating structures have included the

introduction of a phase shift through misalignment of two gratings and the use of blazed gratings to break symmetry.[30,38-40] To optimize the double grating structure, a general design strategy was proposed in which the front grating is treated as an anti-reflection layer to couple incident light while the back grating diffracts light into guided modes to trap it within the thin film.[28,33] The periodicities of both the front and back grating are therefore crucial to the overall performance. However, as these two gratings serve different purposes, they were typically optimized separately in prior studies. For instance, the optimization of the front grating requires striking a balance between larger in-coupling of incident sunlight and decreasing leakage of the guided modes.[24-26,28,33] The period of the back grating is then tuned to further improve light trapping. However, such an optimization can converge to a local maximum, which is determined by the choice of the front grating. To avoid this potential pitfall and simultaneously reduce computational costs of optimization, we propose a more general optimization approach that relies on tuning the periods of two gratings relative to each other, resulting in a simple rule that can be used to design double grating structures to achieve higher absorption in indirect band gap materials.

In this work, we focus on developing an optimized double grating light-trapping structure for a 10-μm-thick c-Si PV cell. Using numerical simulations to solve Maxwell equations, we demonstrate that when a mismatch is introduced between the periods of two gratings, the back grating will diffract incident light into guided modes that couple weakly to the diffraction orders of the front grating. This minimizes the number of incoming solar photons escaping solar cells without getting absorbed, thus improving photocurrent and cell conversion efficiency. By varying the degree of mismatch between the front and back gratings, the highest absorption occurs when the least common multiple (LCM) of the periods between the two gratings is large.

This approach offers more design flexibility and *yields multiple near-optimum designs*, which can be chosen based on the material and fabrication processes. Interestingly, since our approach reveals that the mismatch between two gratings is the most important parameter, optimum designs can have back gratings with either larger or smaller periods than the front grating.

2. Principle

A simple one dimensional (1D) grating based on triangular grooves, in Fig. 1(a), is chosen in this study to act as a 2D analog of inverted nanopyramids or nanocones, which was shown in previous studies to exhibit good light-trapping performance.[15-22,27-28] By using this grating design, it is possible to apply well-established grating theory to better understand the underlying mechanisms and find a design rule to govern light trapping.

In general, gratings are characterized by their dispersion of light into discrete diffraction orders. These orders are determined by adding a characteristic grating momentum, which depends on the period, to the parallel momentum of incoming light,[40]

$$\vec{k}_{2||} = \vec{k}_{1||} + \vec{G}_m \quad (1)$$

where $k_{1||}$ and $k_{2||}$ are parallel wavevectors of the incident and diffracted light respectively, and $\vec{G}_m$ is grating momentum. The subscript ‖ corresponds to the in-plane direction and m is the index for the diffraction order. For the 1D grating in Fig. 1(a), the momentum equation can be simplified as

$$n_2 \frac{2\pi}{\lambda} sin\beta_m = n_1 \frac{2\pi}{\lambda} sin\theta + m\frac{2\pi}{W} \quad (2)$$

where λ is wavelength of light, θ is incident angle, β_m is the diffraction angle for order m, W is the period of the grating, and n_1 and n_2 are refractive indices of air and silicon, respectively. Each diffraction order corresponds to a particular β_m and depends on θ, W, λ, m, and n_2. A drawing of each grating order is shown in Fig. 1(a).

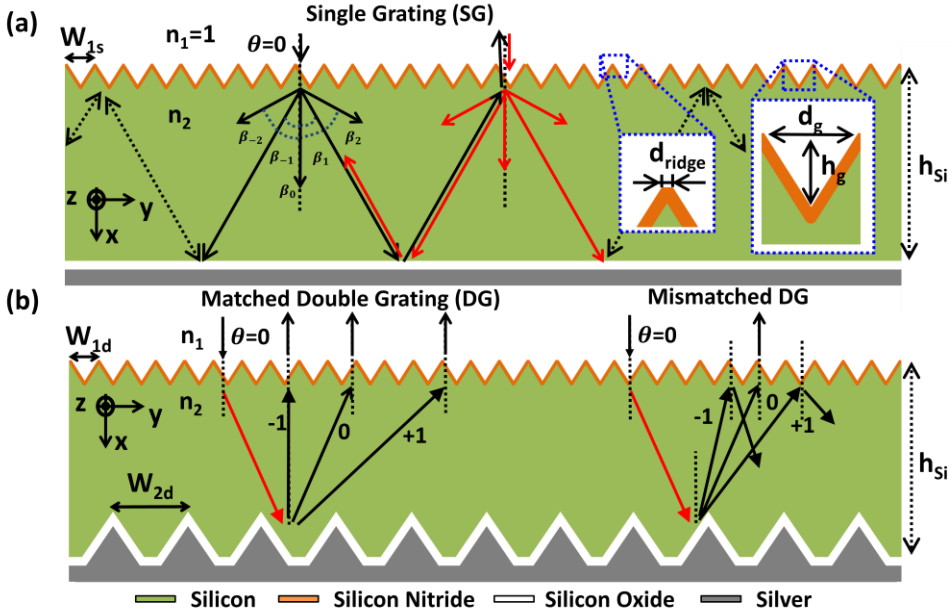

FIG. 1. A schematic of (a) the single grating (SG) case and (b) the double grating case illustrating the design of thin c-Si PV cells. In SG cases, the black and red arrows indicate the different diffraction light is coupled into c-Si by the front grating for the case where W_{1s} = 700 nm and λ = 1000 nm. In DG cases, two grating periods are considered and denoted as W_{1d} and W_{2d} for the front and back gratings respectively. The black and red arrows correspond to the diffraction orders at the wavelength of 1000 nm. *Two cases are considered: the matched DG case where W_{1d} = W_{2d} = 700 nm and mismatched DG case where W_{1d} = 700 nm and W_{2d} = 3100 nm*. The red arrows represent light at normal incidence diffracted into the 1st diffraction order (m = +1) by the front grating. The black arrows represent light diffracted by the back grating. Only the first three diffraction orders (m = -1,0,+1) are shown for both cases; however, there are 11 available diffraction orders (m = -5,-4,-3,-2,-1,0,+1,+2,+3,+4,+5) for this grating structure.

By using a grating to diffract incident light, the addition of the grating momentum along the film plane direction will lead to an increase in the optical path length of light in PV cells as waves propagate more parallel to the film. In addition, for thin c-Si cells, which support guided modes, the diffraction of light also provides greater opportunities to couple into these modes over a broad wavelength range, resulting in improvements in absorption.

In order to further improve light trapping, a second grating is introduced on the back of the PV cell with a period of W_{2d}, as shown in Fig. 1(b). The purpose of the back grating is to add

additional momentum to the diffracted light such that light reflected by the back metal reflector cannot couple back to air through the same diffraction channel. However, it is crucial to note that the addition of a second grating by itself may not lead to better light trapping as improvements will depend on the difference in grating periods, W_{1d} and W_{2d}. For example, if $W_{1d} = W_{2d} = 700$ nm, which corresponds to the optimal grating period in the front single grating (SG) case,[41] the front and back gratings support the same diffraction modes. In this matched double grating (DG) case, the dispersion of the front and back gratings as well as the waveguide modes within the c-Si PV cell are shown in Fig. 2(a). When incident light diffracts into the PV cell by the front grating, it can initially couple into waveguide modes. However, once light reaches the back metal reflector, it is diffracted into the same diffraction order as the front grating, as indicated by the overlap in the dispersion of both grating orders in Fig. 2(a), and it can thus couple back into air. As in the front SG case, unless light is fully absorbed within two passes through the PV cell, these leaky guided modes will allow light to couple back into air.

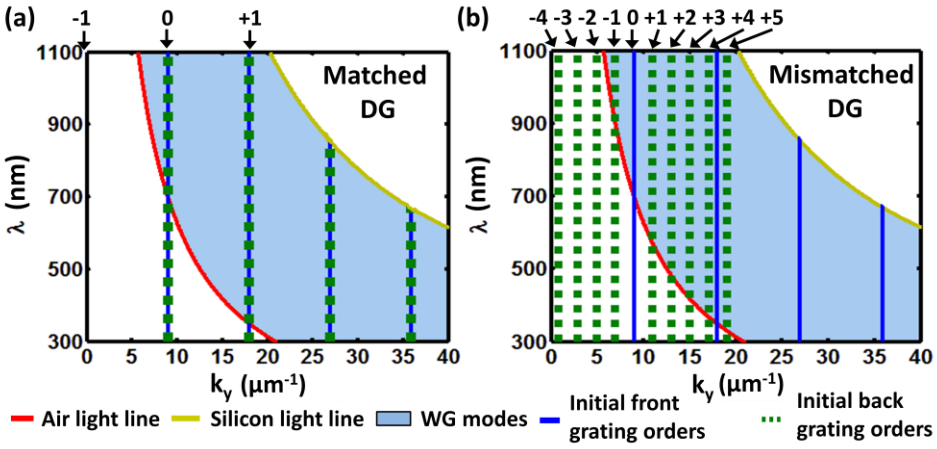

FIG. 2. Waveguide dispersion and diffraction orders are shown in (a) for the matched DG case and (b) for the mismatched DG case. The light line for air is shown in red and light line for c-Si is shown in yellow. The thickness of c-Si is much larger than wavelengths of incident light, thus the density of waveguide modes (WG) is high and their dispersion appears as a continuous light blue region.[41] Diffraction orders of the front and back gratings are shown by the blue vertical lines and dashed green vertical lines, respectively. For simplicity, the diffraction orders shown

correspond to light initially incident on the front and back gratings since subsequent reflections within the c-Si film will result in higher diffraction orders. Furthermore, the diffraction orders of the back grating shown correspond to light incident on the back grating that was diffracted into the m = +1 order of the front grating.

On the other hand, if the periods of both gratings are not matched, light diffracted by the back grating can avoid coupling into diffraction orders of the front grating. For this mismatched DG case, if W_{1d} = 700 nm and W_{2d} = 3100nm, which is a relatively strong mismatch, the dispersion of the grating orders will no longer overlap as shown in Fig. 2(b). As a result, incident light can strongly couple into the guided modes within the PV cell without coupling back into free space. Although it is possible for light to couple back into the front grating orders after multiple diffractions, the effective optical path length can be significantly improved resulting in greater light trapping.

3. Results and discussion

3.1 Numerical proofs for the proposed principle

To assess the light-trapping performance of this grating structure, *numerical finite element electromagnetic simulations (Wave-Optic Module in COMSOL Multiphysics®)* were performed to prove the proposed principle by simulating the SG, matched DG, and mismatched DG cases. As shown in Fig. 1, the system under consideration consists of a thin c-Si absorber with a thickness, h_{Si}, of 10 μm. The triangular grating is used on both sides of PV cells with a height (h_g) to width (d_g) ratio of 0.707, which corresponds to the aspect ratio when monocrystalline {100} silicon is etched with an anisotropic etchant such as potassium hydroxide. A constant ridge width, d_{ridge}, of 50 nm, is included in all grating design to emulate realistic grating structures fabricated in previous studies.[18-19] The total period, W_{1s}, thus equals $W_{1s} = d_g + d_{ridge}$. In addition, a 100-nm-thick silicon nitride antireflection layer is placed on the front of PV cells

to reduce reflection losses. On the backside, a 200-nm-thick silicon dioxide passivation layer and a 300-nm-thick silver back reflector are also included. In these simulations, Floquet boundary conditions are used to simulate an infinitely wide structure. The optical constants of materials were obtained from literatures.[41] For all grating structures, light is assumed to be normally incident and unpolarized, which was calculated by taking the average of the transverse magnetic and transverse electric polarizations.[41]

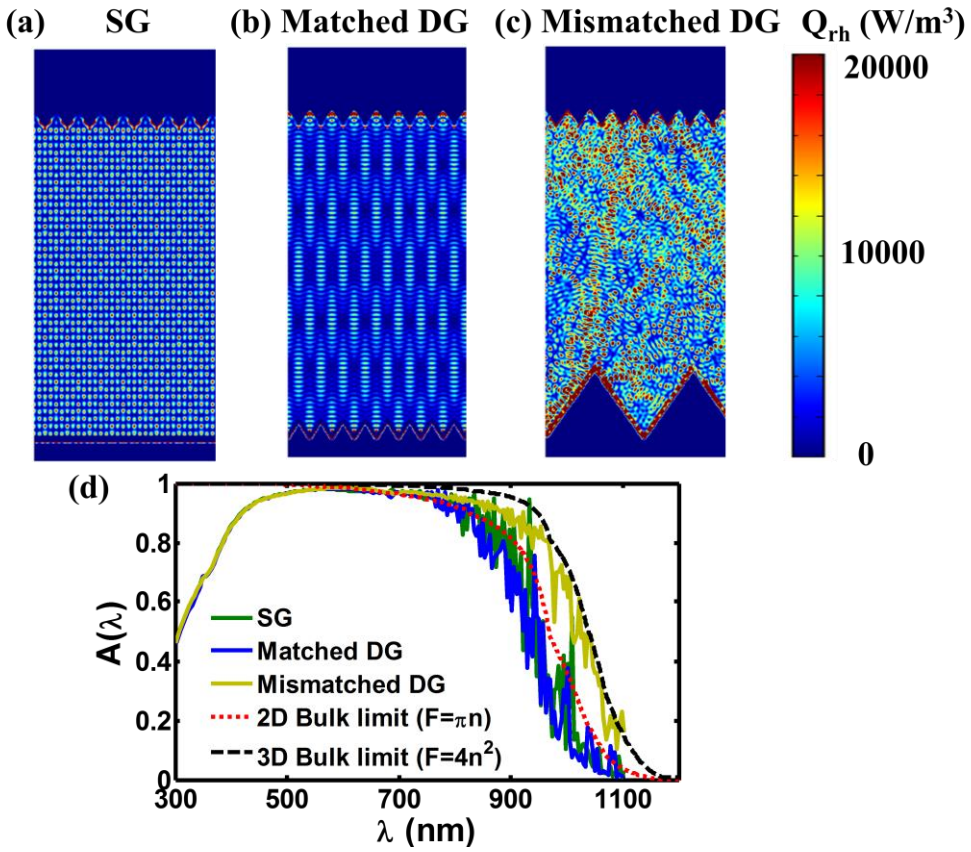

FIG. 3. The spatial distribution of the absorbed intensity, Q_{rh}, for (a) the SG case where W_{1s} = 700 nm, (b) the matched DG case where $W_{1d} = W_{2d} = 700$ nm, and (c) the mismatched DG case where $W_{1d} = 700$ nm and $W_{2d} = 3100$ nm. These Q_{rh} are shown at wavelength, λ, of 1000 nm and a integration bandwidth of 4nm. These pictures are cut, and pictures with their full simulation unit cell are shown in supplementary material.[41] (d) A comparison of absorptance spectra for the SG, matched DG, and mismatched DG cases, as well as 2D and 3D bulk limits.

In Fig. 3, the spatial distribution of absorbed intensity, Q_{rh}, at a wavelength of 1000 nm is shown to visually compare the effects of three cases, and the interference patterns between them are markedly different. In the front SG and matched DG cases, a well-defined interference pattern can be observed, which indicates that light diffracted by the front and back gratings are within phase of each other due to the overlap in diffraction orders. In contrast, in the mismatched DG case, Q_{rh} is more spatially randomized with higher values compared to the other cases. This suggests greater absorption occurs in the mismatched DG case. In addition, absorptance spectra in c-Si for three cases are shown in Fig. 3(d). It can be observed that, in near-IR wavelengths ranged from 800 nm to 1100 nm, the spectral absorptance for the front SG case and the matched DG case are similar, which confirms the earlier intuition that the inclusion of a back grating with a period equal to the front grating does not improve light trapping. For the mismatched DG case, the spectral absorptance clearly exceeds the previous two cases.

3.2 Least common multiple (LCM) rule

Based on the spectral absorptance, the photo-generated current (J_{ph}), which is a more relevant parameter to evaluate the light-trapping performance of PV cells, is calculated using the following expression, $J_{ph} = \int_0^{\lambda_g} A(\lambda) I_{AM1.5G}(\lambda) \frac{q\lambda}{hc} d\lambda$, where A is spectral absorptance, $I_{AM1.5G}$ is intensity of AM1.5G solar spectrum, λ_g is the corresponding wavelength of bandgap, q is the elementary charge, h is the Planck constant, and c is the speed of light in vacuum.

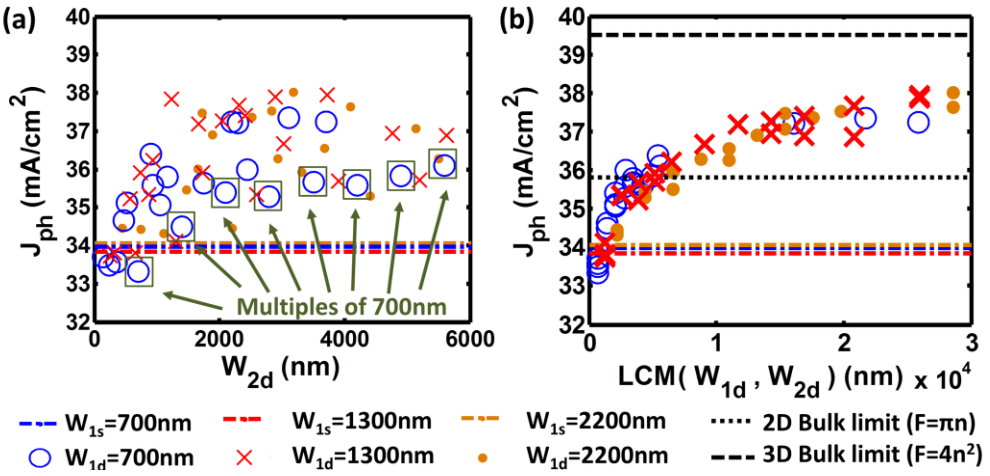

FIG. 4. Double grating (DG) results. Simulations were performed at normal incidence (θ=0°) and h_{Si}=10μm. (a) The photo-generated current (J_{ph}) as a function of the back grating period (W_{2d}) assuming front grating periods of W_{1s} = 700 nm, 1300 nm, and 2200 nm. (b) J_{ph} as a function of the least common multiple, LCM(W_{1d},W_{2d}). In both (a) and (b), single grating cases with front grating periods of W_{1s} = 700 nm, 1300 nm, and 2200 nm and 2D and 3D bulk limits are shown for comparison.

Using the expression, J_{ph} is plotted as a function of the back grating period (W_{2d}) assuming the front grating period is W_{1d} = 700 nm, 1300 nm, and 2200 nm, as shown in Fig. 4(a) at normal incidence. The results for the front SG case assuming W_{1s} = 700 nm, 1300 nm, and 2200 nm are plotted for comparison.[41] As shown, J_{ph} exhibits an overall increase with W_{2d}, but with an oscillatory behavior that exhibits local minima at multiples of W_{1d}. This suggests that, even with a large mismatch in the front and back grating periods, light can still efficiently couple into diffraction orders of the front grating if W_{2d} is a higher multiple of W_{1d}. For example, in Fig. 4(a), the case of W_{1d} = 700 nm has lower J_{ph} while W_{2d} is a multiple of W_{1d}.

To show the impact of this effect, J_{ph} is plotted as a function of the least common multiple (LCM) of W_{1d} and W_{2d} in Fig. 4(b). As shown, J_{ph} now exhibits a clear trend of monotonically exponential saturation. This is due to absorption occurring as an exponential decay in accordance to the Beer-Lambert law.[42] To show this dependence, J_{ph} can be expressed in terms of the optical

path length of light, ℓ, as follows, $J_{ph} = \int_0^{\lambda_g} I_\lambda (1 - e^{-\alpha_\lambda \ell_\lambda}) \frac{q\lambda}{hc} d\lambda$, where I_λ is spectral intensity of light upon entering the absorber, and α_λ is the absorption coefficient. From this expression, J_{ph} will saturate when ℓ_λ is sufficiently large, which coincides with the trend shown in Fig. 4(b). Based on these results, the LCM can be used to determine the optimal mismatch between the front and back grating periods, thus providing a means to maximize light trapping in double grating systems. Based on the various cases in Fig. 4(b), the highest J_{ph} found at *normal incidence* is 38.02 mA/cm^2 corresponding to W_{1d} = 2200 nm, W_{2d} = 3177.78 nm ($W_{2d} = \frac{13}{9} W_{1d}$), and a LCM = 28600 nm. This value is nearly 4 mA/cm^2, or 11.76%, higher than the optimal front SG case ($J_{ph} \approx$ 34 mA/cm^2)[41] and exceeds the 2D bulk limit ($F=\pi n$). However, it does not exceed the 3D bulk limit, which is also known as the Yablonovitch or Lambertian limit ($F=4n^2$), where absorptance spectra are given by $A(\lambda) = \alpha_\lambda h_{Si}/(\alpha_\lambda h_{Si} + 1/F)$ with F the enhancement factor.[24-26,28,43] To properly compare our results with the bulk limits, angular dependence of these structures was also investigated in section 3.4. Additionally, it should be noted that an increase in the grating period will lead to greater removal of the absorbing medium and modification of guided modes from the planar thin film. Thus, it is possible to achieve different J_{ph} and deviate from the exponential saturation curve for the same LCM. For example, if W_{1d} = 2200 nm, J_{ph} = 37.64 mA/cm^2 when W_{2d} = 4085.7 nm ($W_{2d} = \frac{13}{7} W_{1d}$) and J_{ph} = 38.02 mA/cm^2 when W_{2d} = 3177.8 nm ($W_{2d} = \frac{13}{9} W_{1d}$), despite the fact that both cases exhibit an LCM equal to 28,600 nm.

3.3 Dependency on crystalline silicon film thickness

To understand the effect of the crystalline silicon film thickness (h_{Si}) for various least common multiple front and back gratings, additional simulations were performed for h_{Si} = 2μm, 5μm, and 10μm. The photogenerated current (J_{ph}) is plotted as a function of the least common

multiple parameter in Fig. 5. The front period is fixed to be W_{1d} = 700nm for all three cases. At these three thicknesses, the photogenerated currents generally increase with their least common multiple following an exponential saturation trend. For the 2-μm-thick case, the J_{ph} decreases at a very large least common multiple due to excess removal of material from the silicon absorber leading to poor absorption. The single grating case with a front grating period of W_{1s} = 700 nm, the 2D bulk limit (F=πn), and the 3D bulk limit ($F=4n^2$) are also shown for comparison.

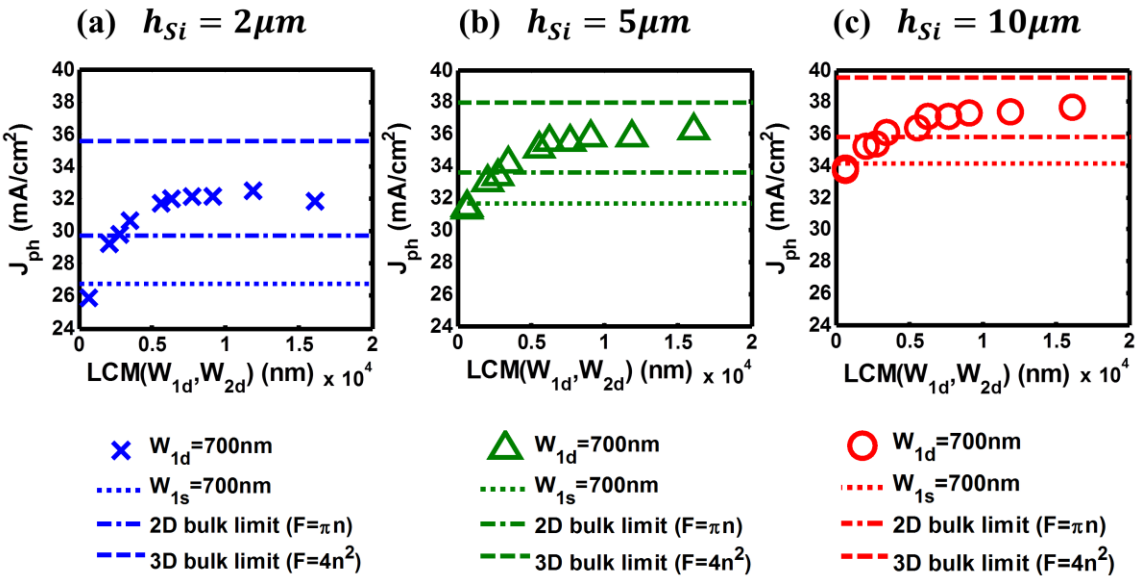

FIG. 5. Double grating (DG) results for various thickness of crystalline silicon absorber (h_{Si}). Simulations were performed at normal incidence (θ=0°) and W_{1d}=700nm. The photo-generated current (J_{ph}) as a function of the least common multiple, LCM(W_{1d},W_{2d}) are shown with h_{Si} = 2μm in (a), h_{Si} = 5μm in (b), and h_{Si} = 10μm in (c). In (a), (b), and (c), the single grating cases with front grating periods of W_{1s} = 700 nm, 2D bulk limit (F=πn), and 3D bulk limit ($F=4n^2$) are shown for comparison.

3.4 Angular dependence

To compare the most optimal DG structure based on the LCM design rule (J_{ph} = 38.02 mA/cm^2, W_{1d} = 2200 nm, W_{2d} = 3177.78 nm ($W_{2d} = \frac{13}{9} W_{1d}$), and LCM = 28,600 nm.) to the 2D bulk limit,[24-26] further simulations were performed to evaluate the absorptance for incident angles ranging from 0^o to 90^o as plotted in Fig. 6a. As shown, the SG, matched DG, and mismatched DG cases all exhibit a similar angular dependence, due to the same top grating structure, with a minor decrease in absorptance up to an angle of incidence about 50 degrees after which the absorptance decreases significantly. This sudden decrease is due to light at large angles of incidence observing the grating structure as a planar surface. Based on the aspect ratio of the triangular grating in our simulation, this transition occurs at approximately 54.73^o. As a result, the angle-averaged absorptance is lower than at normal incidence, as shown in Fig. 6b. However, for the mismatched DG case, the angle-averaged absorptance can still achieve a significantly higher absorptance from 965 nm to 1100 nm compared to the SG and the matched DG cases. In fact, within these wavelengths, the angle-averaged mismatched DG case also exceeds the 2D bulk limit. To understand the reason, it is important to recall that the bulk limit was derived assuming the photon density of state (DOS) for a bulk medium. For a thin film, the DOS can deviate dramatically since the guided modes supported in the film exhibit a flat dispersion near the cut-off frequency of the mode.[24,44-46] This can result in a photon DOS that exceeds the DOS of a bulk medium, thus enabling a thin PV cell to potentially exceed the ray optics or bulk limit.

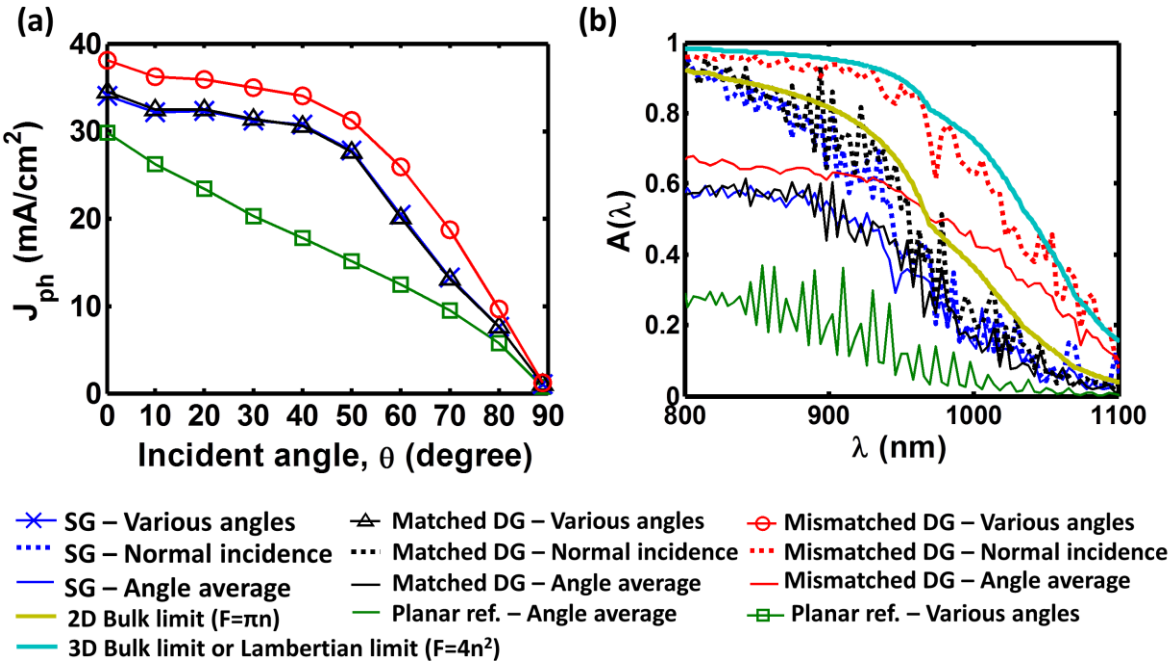

FIG. 6. (a) The angular dependence of J_{ph} for each case at various angles from 0^o to 90^o were computed for the SG case (W_{1s} = 2200 nm), matched DG case (W_{1d} = W_{2d} = 2200 nm), and mismatched DG case (W_{1d} = 2200 nm and W_{2d} = 3177.78 nm). (b) The angle-averaged absorptances of three cases were in comparison with the 2D bulk limit and 3D bulk limit (Lambertian limit).

3.5 Generalization of the LCM rule

This design methodology is also not restricted to only PV, but can be applied to any materials in different applications such as photodetectors. As an example, the LCM design rule was also applied to a 3-μm-thick germanium (Ge) film, which is a common material used for near-IR photodetectors. In general, Ge weakly absorbs light in the 1.5 to 1.65 μm wavelength range. By applying the same grating structure to this film, we show that the spectral absorptance can again be dramatically improved for an optimally mismatched DG structure in Fig. 7.

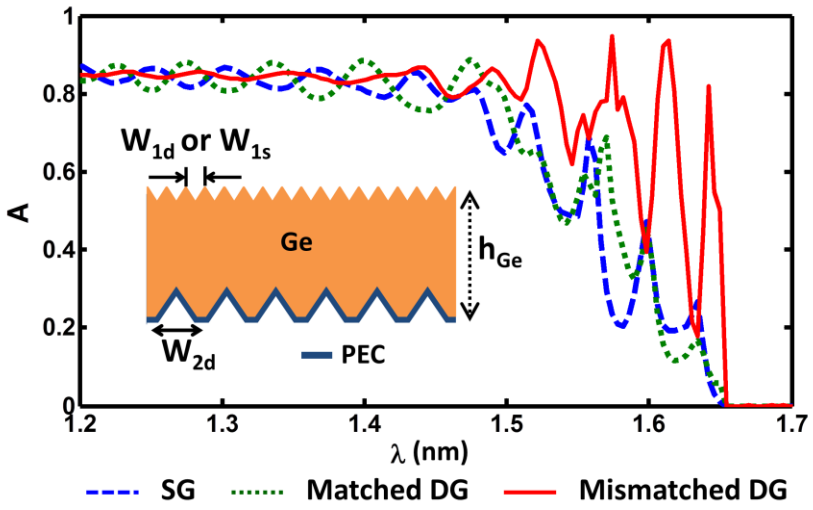

FIG. 7. The LCM design rule is general and can be applied to any material. As a demonstration, the LCM design rule is applied to a thin Ge film with a thickness of h_{Ge} = 3 μm (inset). The absorptance spectra is shown for the SG case (W_{1s} = 700 nm), the matched DG case (W_{1d} = W_{2d} = 700 nm), and the mismatched DG case (W_{1d} = 700 nm and W_{2d} = 1100 nm). PEC is the boundary condition of perfect electric conductor.

Another important point is that the LCM rule can be directly applied to 3D PV cells using 2D gratings. The improvement to light trapping that we propose is purely dependent on the ratio of the front and back grating periods. From Eq. (1), 2D gratings would provide lattice momentum along two orthogonal directions. This means that 2D gratings can be viewed as a combination of two 1D gratings. Thus, it is expected that the light-trapping performance for 3D PV cells using 2D grating structures on the front and back sides will also be significantly improved. One should be noted that the shape of the gratings such as a rectangle and trigon, the proposed least common multiple rule will also yield optimized optical designs. Different symmetries of the gratings (both in one and two dimensions) can serve as additional fitting parameters to produce even more optimal thin-film PV cell designs.

3.6 Limitation of the LCM rule

Direct implementation of the LCM rule yields a large LCM value for a double-grating design with two similar periods on the front and back gratings. However, there is a limitation

using LCM rule in this situation, which stems from the finite angle width ($\Delta\beta_m$) of the discrete grating channels. When the periods of the front and back gratings are very close to each other, the diffraction orders of the front grating will overlap with the diffraction orders of the back grating, causing the leakage of light and a breakdown of the LCM rule. The finite angle width of a grating channel can be calculated using Eq. (2). For example, a case with W_{1s} = 700 nm, λ=1000 nm, n_2=3.588, and m = -1, and the $\Delta\beta_{-1} = (\beta_{-1})^{+} - (\beta_{-1})^{-} = 42.60^{o} - 23.46^{o} = 19.14^{o}$.

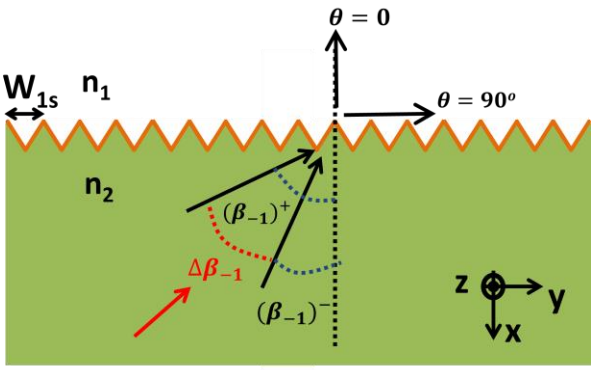

FIG. 8. The angle width ($\Delta\beta_m$) of the grating channel. The finite angle width of the grating channel will cause to the breakdown of the least common multiple rule when periods of the front and back gratings are too close to each other.

4. Conclusion

To summarize, light trapping and absorption in thin c-Si PV cells can be dramatically improved by using a front and back grating with mismatched periods. To facilitate the design of a double grating structure, we propose the least common multiple (LCM) design rule, which provides a simple method to determine the optimal mismatch between periods of two gratings in order to increase light absorption. To illustrate this rule, we optimized the front and back grating periods for a thin 10-μm-thick c-Si PV cell and show that it yields several optimal designs, which deviate from previous studies that predict the existence of a single optimal design for a double grating structure.[28,30] For example, a double grating structure designed with this rule is

predicted to increase the photo-generated current for a 10-μm-thick c-Si PV cell from ~34.0 mA/cm^2 for a single front grating to 38.02 mA/cm^2 for a double-grating case at normal incidence. Even when averaged over the incident angle from 0^o to 90^o, the optimal mismatched DG case can still achieve an absorptance that exceeds the fundamental 2D bulk limit in the wavelength range from 965 nm to 1100 nm. This design rule is general and can be applied to any indirect band gap material such as germanium, which is commonly used in near-infrared photodectors. Given the simplicity of the proposed design strategy and its compatibility with standard manufacturing techniques, the mismatched double grating design can enable significant improvements to device performance as well as other optoelectronic devices such as photodetectors.

AUTHOR INFORMATION

Corresponding Authors

a)E-mail: sborisk@mit.edu (S. V. Boriskina)

b)E-mail: gchen2@mit.edu (G. Chen)

ACKNOWLEDGMENT

The authors gratefully acknowledge the discussions with Professor Nicholas X. Fang, the Massachusetts Institute of Technology, USA. This work was supported by DOE-BES, funded by the US Department of Energy, Office of Science, and Office of Basic Energy, Award No. DE-SC0001299/DE-FG02-09ER46577 for fundamental research in light management, and the U.S. Department of Energy Sunshot Initiative, Award No. DE-EE0005320 for high-efficiency thin-film c-Si PV cell design.

REFERENCES

[1] W. Shockley, H. J. Queisser, Detailed balance limit of efficiency of pn junction solar cells, *J. Appl. Phys.* **32** (1961) 510-519.

[2] D.M. Powell, M. T. Winkler, A. Goodrich, T. Buonassisi, Modeling the cost and minimum sustainable price of crystalline silicon photovoltaic manufacturing in the United States, *IEEE J. Photovolt* **3** (2013) 662–668.

[3] D. M. Powell, M. T. Winkler, H. J. Choi, C. B. Simmons, D. Berney Needleman, T. Buonassisi, Crystalline silicon photovoltaics: a cost analysis framework for determining technology pathways to reach baseload electricity costs, *Energy Environ. Sci.* **5** (2012) 5874.

[4] SEMI. International Technology Roadmap for Photovoltaic (ITRPV), 5th Ed. < http://www.itrpv.net/.cm4all/iproc.php/Reports%20downloads/ITRPV_2014_Roadmap_Revision1_140324.pdf?cdp = a> **2014**.

[5] J. H. Petermann, D. Zielke, J. Schmidt, F. Haase, E. G. Rojas, R. Brendel. 19%-efficient and 43μm-thick crystalline Si solar cell from layer transfer using porous silicon, *Prog. Photovolt: Res. Appl.* **20** (2012) 1-5.

[6] R. Brendel. Review of layer transfer processes for crystalline thin-film silicon solar cells, *Jpn. J. Appl. Phys*. **40** (2001) 4431-4439.

[7] R. Brendel, Thin-film crystalline silicon mini-modules using porous Si for layer transfer, *Solar Energy* **77** (2004) 969–982.

[8] M. LaMonica, 1366 Technologies. *MIT Tech. Rev.* <http://www.technologyreview.com/featuredstory/524551/solar-survivor/> (2014).

[9] X. Li, N. P. Hylton, V. Giannini, K.-H. Lee, N. J. Ekins-Daukes, S. A. Maier, Multi-dimensional modeling of solar cells with electromagnetic and carrier transport calculations, *Prog. Photovolt: Res. Appl.* **21** (2013) 109-120.

[10] M. G. Deceglie, V. E. Ferry, A. P. Alivisatos, H. A. Atwater, Design of nanostructured solar cells using coupled optical and electrical modeling, *Nano Lett*. **12** (2012) 2894-2900.

[11] S. Pillai, K. R. Catchpole, T. Trupke, M. A. Green, Surface plasmon enhanced silicon solar cells, *J. Appl. Phys*. **101** (2007) 093105.

[12] L. Zeng, P. Bermel, Y. Yi, B. A. Alamariu, K. A. Broderick, J. Liu, C. Hong, X. Duan, J. Joannopoulos, L. C. Kimerling, Demonstration of enhanced absorption in thin film Si solar cells with textured photonic crystal back reflector, *Appl. Phys. Lett*. **93** (2008) 221105.

[13] X. Sheng, J. Liu, I. Kozinsky, A. M. Agarwal, J. Michel, L. C. Kimerling, Design and non-lithographic fabrication of light trapping structures for thin film silicon solar cells, Adv. Mater. **23** (2011) 843-847.

[14] P. Bermel, C. Luo, L. Zeng, L. C. Kimerling, J. D. Joannopoulos, Improving thin-film crystalline silicon solar cell efficiencies with photonic crystals, *Opt. Express* **15** (2007) 16986-17000.

[15] V. K. Narasimhan, Y. Cui, Nanostructures for photon management in solar cells, Nanophotonics **2** (2013) 187-210.

[16] S. Jeong, S. Wang, Y. Cui, Nanoscale photon management in silicon solar cells, J. Vac. Sci. Technol. A 3 (2012) 06080.

[17] M. L. Brongersma, Y. Cui, S. Fan, Light management for photovoltaics using high-index nanostructures, *Nature Mat*., **13** (2014) 451-460.

[18] M. S. Branham, W.-C. Hsu, S. Yerci, J. Loomis, S. V. Boriskina, B. R. Hoard, S. E. Han, G. Chen, 15.7% Efficient 10-μm-thick crystalline silicon solar cells using periodic nanostructures, *Adv. Mater*. **27** (2015) 2182-2188.

[19] A. Mavrokefalos, S. E. Han, S. Yerci, M. S. Branham, G. Chen, Efficient light trapping in inverted nanopyramid thin crystalline silicon membranes for solar cell applications, *Nano Lett.* **12** (2012) 2792–2796.

[20] S. E. Han, G. Chen, Toward the Lambertian limit of light trapping in thin nanostructured silicon solar cells, *Nano Lett.* **10** (2010) 4692-4696.

[21] L. A. Weinstein, W.-C. Hsu, S. Yerci, S. V. Boriskina, and G. Chen, Enhanced absorption of thin-film photovoltaic cells using an optical cavity, *J. Opt.* **17** (2015) 055901.

[22] S. Jeong, M. D. McGehee, Y. Cui, All-back-contact ultra-thin silicon nanocone solar cells with 13.7% power conversion efficiency, *Nat. Comm.* **4** (2013) 2950.

[23] M. D. Kelzenberg, S. W. Boettcher, J. A. Petykiewicz, D. B. Turner-Evans, M. C. Putnam, E. L. Warren, J. M. Spurgeon, R. M. Briggs, N. S. Lewis, H. A. Atwater, Enhanced absorption and carrier collection in Si wire arrays for photovoltaic applications, *Nat. Mater.* **9** (2010) 239–244.

[24] Z. Yu, A. Raman, S. Fan, Fundamental limit of nanophotonic light trapping in solar cells, *Proc. Natl. Acad. Sci. U.S.A.* **107** (2010) 17491-17496.

[25] Z. Yu, A. Raman, S. Fan, Fundamental limit of light trapping in grating structures, *Opt. Express* **10** (2010) A366-A380.

[26] K. X. Wang, Z. Yu, V. Liu, A. Raman, Y. Cui, S. Fan, Light trapping in photonic crystals. *Energy Environ. Sci.* **7** (2014) 2725.

[27] C.-M. Hsu, C. Battaglia, C. Pahud, Z. Ruan, F.-J. Haug, S. Fan, C. Ballif, Y. Cui, High-efficiency amorphous silicon solar cell on a periodic nanocone back reflector, *Adv. Energy Mater.* **2** (2012) 628–633.

[28] K. X. Wang, Z. Yu, V. Liu, Y. Cui, S. Fan, Absorption enhancement in ultrathin crystalline silicon solar cells with antireflection and light-trapping nanocone gratings, *Nano Lett.* **12** (2012) 1616–1619.

[29] A. Ingenito, O. Isabella, M. Zeman, Experimental demonstration of 4n2 classical absorption limit in nanotextured ultrathin solar cells with dielectric omnidirectional back reflector, *ACS Photonics* **1** (2014) 270-278.

[30] A. Abass, K. Q. Le, A. Alu, M. Burgelman, B. Maes, Dual-interface gratings for broadband absorption enhancement in thin-film solar cells, *Phys. Rev. B* **85** (2012) 115449.

[31] W. Zhang, L. Jiang, X. Li, Broadband light harvesting enhancement with front double and back metallic gratings in thin film solar cells, *Opt. Comm.* **317** (2014) 83-87.

[32] M. Zeman, O. Isabella, S. Solntsev, K. Jager, Modelling of thin-film silicon solar cells, *Solar Energy Materials & Solar Cells* **119** (2013) 94-111.

[33] X. Meng, E. Drouard, G. Gomard, R. Peretti, A. Fave, C. Seassal, Combined front and back diffraction gratings for broad band light trapping in thin film solar cell, *Opt. Express* **20** (2012) A561-A571.

[34] P. Wang, R. Menon, Optimization of periodic nanostructures for enhanced light-trapping in ultra-thin photovoltaics, *Opt. Express* **21**, (2013) 6274-6285.

[35] C. S. Schuster, P. Kowalczewski, E. R. Martins, M. Patrini, M. G. Scullion, M. Liscidini, L. Lewis, C. Reardon, L. C. Andreani, T. F. Krauss, Dual gratings for enhanced light trapping in thin-film solar cells by a layer-transfer technique, *Opt. Express* **21** (2013) A433-A438.

[36] B. Shen, P. Wang, R. Menon, Optimization and analysis of 3D nanostructures for power-density enhancement in ultra-thin photovoltaics under oblique illumination, *Opt. Express* **22**, (2014) A311-A319.

[37] R. Dewan, D. Knipp, Light trapping in thin-film silicon solar cells with integrated diffraction grating, *J. Appl. Phys*. **106** (2009) 074901 (2009).

[38] Z. Xia, Y. Wu, R. Liu, Z. Liang, J. Zhou, P. Tang, Misaligned conformal gratings enhanced light trapping in thin film silicon solar cells, *Opt. Express* **21** (2013) A548-A557.

[39] A. Chutinan, C. W. W. Li, N. P. Kherani, S. Zukotynski, Wave-optical studies of light trapping in submicrometre-textured ultra-thin crystalline silicon solar cells, *J. Phys. D: Appl. Phys*. **44** (2011) 262001.

[40] S. Mokkapati, K. R. Catchpole, Nanophotonic light trapping in solar cells, *J. Appl. phys*. **112** (2012) 101101.

[41] Supplemental material. **Section I** shows absorption profile of 10-μm-thick c-Si and absorption depths of c-Si. **Section II** shows waveguide modes in crystalline silicon. **Sections III** shows optical constants of materials for simulated solar cells. **Section IV** shows absorptance of transverse magnetic and transverse electric polarized light. **Section V** shows profiles of absorbed intensity, electric fields, and magnetic fields for various light-trapping cases. **Section VI** shows all combination of W_{1d} and W_{2d} in Fig. 4.

[42] M. F. Modest, *Radiative Heat Transfer*; McGraw-Hill: New York (1993).

[43] V. Ganapati, O. D. Miller, E. Yablonovitch, Light trapping textures designed by electromagnetic optimization for subwavelength thick solar cells, *IEEE J. Photovolt*. **4** (2014) 175-182.

[44] H. R. Stuart, D. G. Hall, Thermodynamic limit to light trapping in thin planar structures, *J. Opt. Soc. Am. A* **14** (1997) 3001-3008.

[45] D. M. Callahan, J. N. Munday, H. A. Atwater, Solar cell light trapping beyond the ray optic limit, *Nano Lett*. **12** (2012) 214-218.

[46] S. V. Boriskina, H. Ghasemi, G. Chen, Plasmonic materials for energy: from physics to applications, *Materials Today* **16** (2013) 379-390.

Supplementary Material

Mismatched Front and Back Gratings for Optimum Light Trapping in Thin Crystalline Silicon Solar Cells

Wei-Chun Hsu,[†] Jonathan K. Tong,[†] Matthew S. Branham,[†] Yi Huang,[†] Selçuk Yerci,[†,‖] Svetlana V. Boriskina,[†,a)] and Gang Chen[†,b)]

[†]*Department of Mechanical Engineering, Massachusetts Institute of Technology, Cambridge, Massachusetts 02139, USA*

[‖]*Micro and Nanotechnology Programme, Electric and Electronics Engineering, and the Center for Solar Energy Research and Applications, Middle East Technical University, Ankara 06800, Turkey.*

Corresponding Authors

a)E-mail: sborisk@mit.edu (S. V. Boriskina)

b)E-mail: gchen2@mit.edu (G. Chen)

Section I. Spectral Absorptances and Photo-Generated Current of Single Grating (SG)

The spectral absorptances of the front SG structure for various periods are shown in Fig. S1b, which were obtained by normalizing the intensity of the absorbed light, $Q_{rh}(\lambda)$, to $I_{AM1.5G}(\lambda)$. Overall, the spectral absorptance is enhanced as the period, $W_{1s,}$ increases. In the short wavelength range between 300 nm and 500 nm, the spectral absorptance is much lower than unity due to a combination of a shallow penetration depth and absorption losses in the silicon nitride antireflection layer. Additionally, the relative planar area of the cell, which is due to the finite ridge width, will decrease as W_{1s} increases resulting in a higher absorptance. The kink in the spectral absorptance at a wavelength of 360 nm can be attributed to interband transitions in silicon, which lead to a sharp change in the optical constants. In the near-IR wavelength range between 800 nm and 1100 nm, a larger grating period leads to a higher spectral absorptance. This can be attributed to a reduction in the reflection loss and an increase in path length since more diffraction modes are supported when W_{1s} increases.

To better visualize the impact of the period, W_{1s}, on light-trapping performance, Fig. S1c shows the photo-generated current based on the spectra shown in Figure S1b. As shown, an increase in the grating period leads to a higher J_{ph}, which follows the insight obtained from the grating analysis. However, this enhancement does not persist as it can be observed that for grating periods larger than 700 nm, J_{ph} begins to saturate. When W_{1s} is much larger than the wavelength of light, the grating no longer diffracts incident light, but rather interacts with light in the ray optics regime where it locally refracts light based on the angle of the grooves. The subtle variations in J_{ph} as the period increases further is due to the change in the volume of absorbing silicon and strong oscillation of spectral absorptance in the wavelength range of 700 ~ 1100 nm.

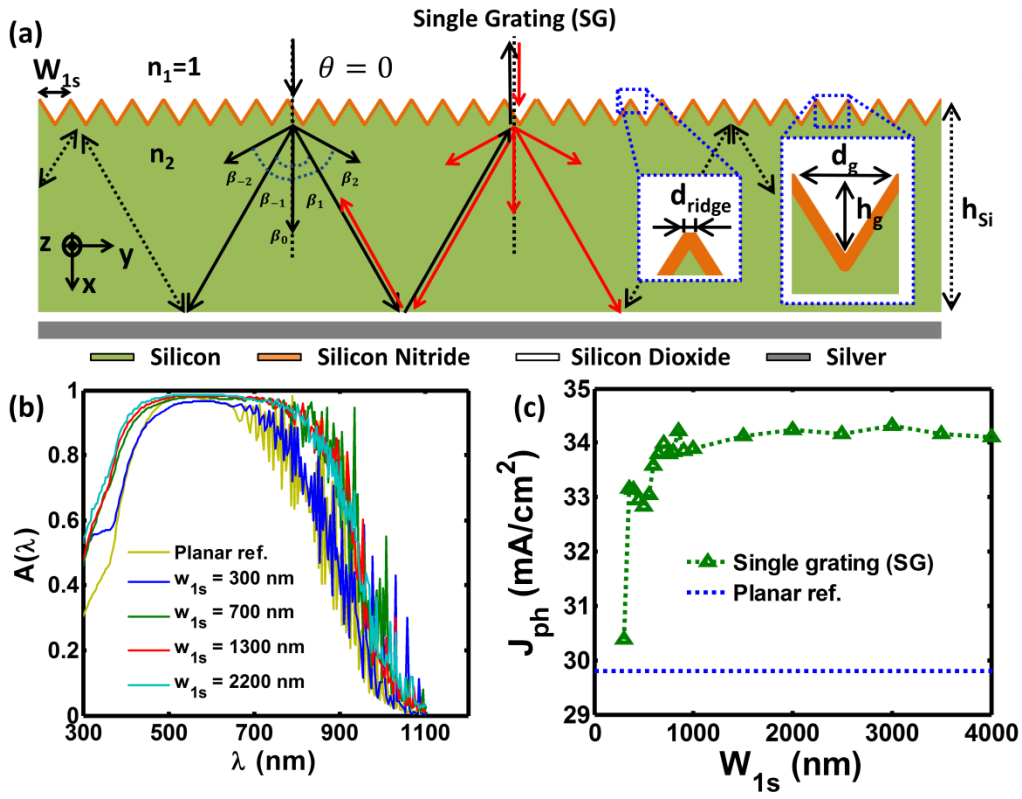

FIG. S1. The single grating (SG) case. (a) A schematic illustrating the design of the thin c-Si PV cell. The grating consists of triangular grooves with a height (h_g) to width (d_g) ratio of h_g/d_g = 0.707. Each groove has a ridge width, d_{ridge} = 50 nm. Thus, the total grating period is $W_{1s} = d_g - d_{ridge}$. The silicon layer has thickness, h_{Si}, of 10 μm before etching. A 100-nm-thick silicon nitride antireflection layer is included on top of silicon after grating structures are formed. On the back of the PV cell, a 200-nm-thick silicon dioxide passivation layer and a 300-nm-thick silver back reflector is included. Simulations were performed at normal incidence (θ=0) for both TM and TE polarizations. The black and red arrows indicate the different diffraction light will couple into when diffracted by the front grating for the case where W_{1s} = 700 nm and λ = 1000 nm. (b)The absorptance spectra for various W_{1s}. For comparison, the absorptance spectrum of a planar PV cell with a 70-nm-thick silicon nitride antireflection layer is plotted. (c) The corresponding photo-generated current (J_{ph}) for various W_{1s} as well as a planar reference cell.

Section II. Waveguide Modes in Crystalline Silicon

Dispersions of crystalline silicon waveguide are shown in this section. Since there is a bottom silver mirror, thickness of a symmetric waveguide is approximate twice thickness of silicon, h_{Si}, absorber. Fig. S2(a) shows a conventional way to plot dispersion in terms of frequency of photons with h_{Si} = 1 μm. Left bound (red line) is light line of air, and right bound (yellow line) is light line of crystalline silicon. Waveguide modes are reasonable to exist between these two light lines, and transverse electric (TE) even modes, TE odd modes, transverse (TM) even modes, and TM odd modes are plotted.[1] In this paper, dispersion is plotted in terms of wavelengths of photons for convenience of discussion, so Fig. S2(a) is re-plotted to be Fig. S2(b). When silicon thickness is reduced to h_{Si} = 100 nm, discrete modes at a given wavelength can be clearly observed in Fig. S2(c). However, when silicon thickness increase to h_{Si} = 10 μm, density of waveguide modes is very high (Fig. S2(d)). Therefore, we mark waveguide modes as a light blue region in Fig. 2(a) and Fig. 2(b).

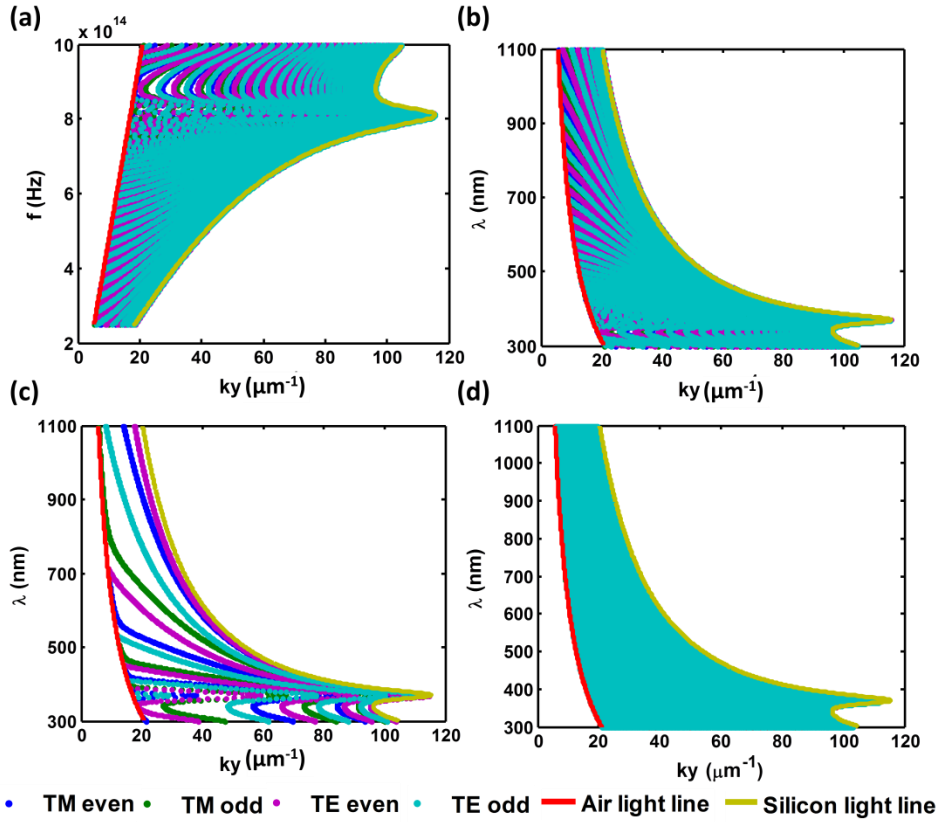

FIG. S2. Dispersion of the symmetric waveuguide modes of crystalline silicon. Due to a mirror on the bottom silicon absorber, thickness of waveguide is approximate twice the thickness of silicon, h_{Si}. k_y is the parallel wavevector along the y direction of waveguide. (a) Thickness of silicon is 1μm, and the dispersions are plotted in terms of frequency of photons. (b) Thickness of silicon is 1μm, and the dispersions are plotted in terms of wavelength of photons. (c) Thickness of silicon is 100nm. (d) Thickness of silicon is 10μm.

Section III. Optical Constants of Materials for Simulated Solar Cells

Optical constants, real and imaginary parts of refractive index, of chosen material for simulated solar cell of thin crystalline silicon (c-Si) are shown. Fig. S3 shows real and imaginary parts of optical constants of plasma-enhanced chemical vapour deposition silicon nitride in Fig. S3(a) and S3(b),[2] crystalline silicon in Fig. S3(c) and S3(d),[3-4] silicon dioxide in Fig. S3(e) and S3(f),[5] silver in Fig. S3(g) and S3(h),[6] and germanium in Fig. S3(g) and S3(h).[7]

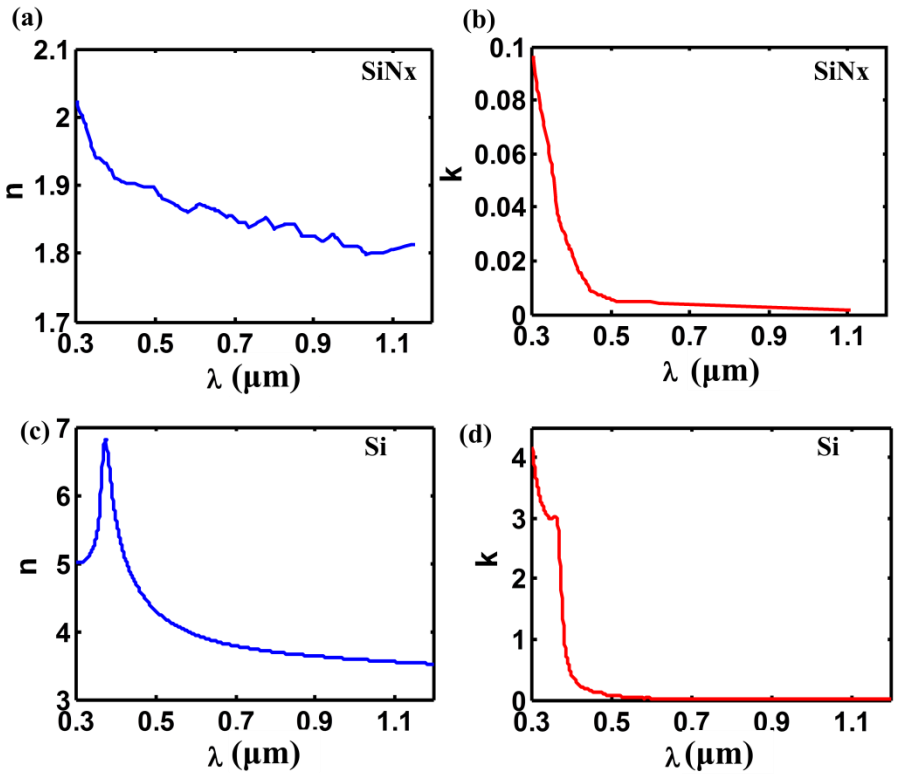

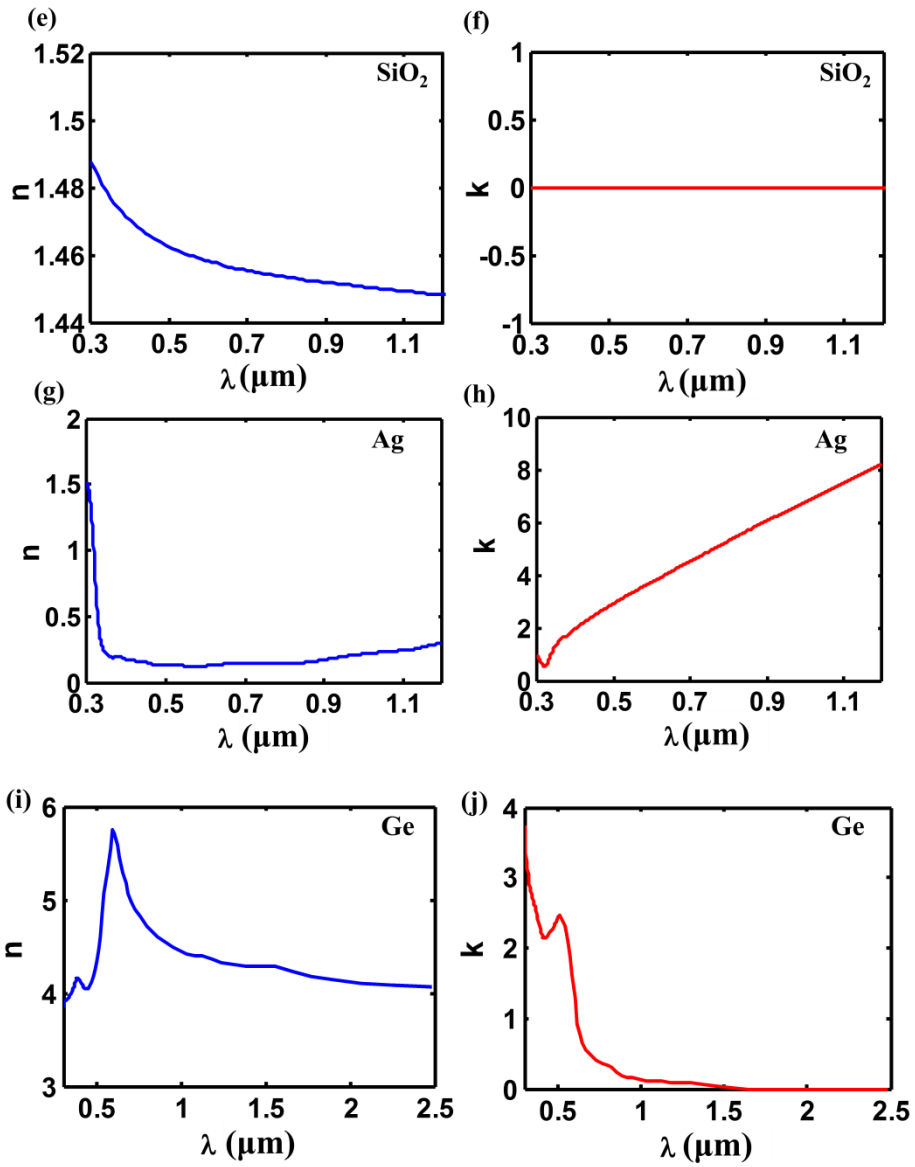

FIG. S3. Optical constants used in numerical simulations. (a) and (b) are real and imaginary parts of plasma-enhanced vapour deposition silicon nitride respectively. (c) and (d) are real and imaginary parts of crystalline silicon. (e) and (f) are real and imaginary parts of silicon dioxide. (g) and (h) are real and imaginary parts of silver. (i) and (j) are real and imaginary parts of germanium.

Section IV. Absorptance of Transverse Magnetic and Transverse Electric Polarized Light

Absorptances using transverse magnetic (TM) and transverse electric (TE) polarized light are calculated separately for the single grating (SG) structure in Fig. 1(a). A 100-nm-thick antireflective silicon nitride, 10-μm-thick c-Si, 200-nm-thick silicon dioxide, and 300-nm-thick silver are used. For normal incident light, absorptances of two polarized light do not differ significantly from each other, so absorptances of unpolarized light can be approximated by taking average of values of TM and TE fields.

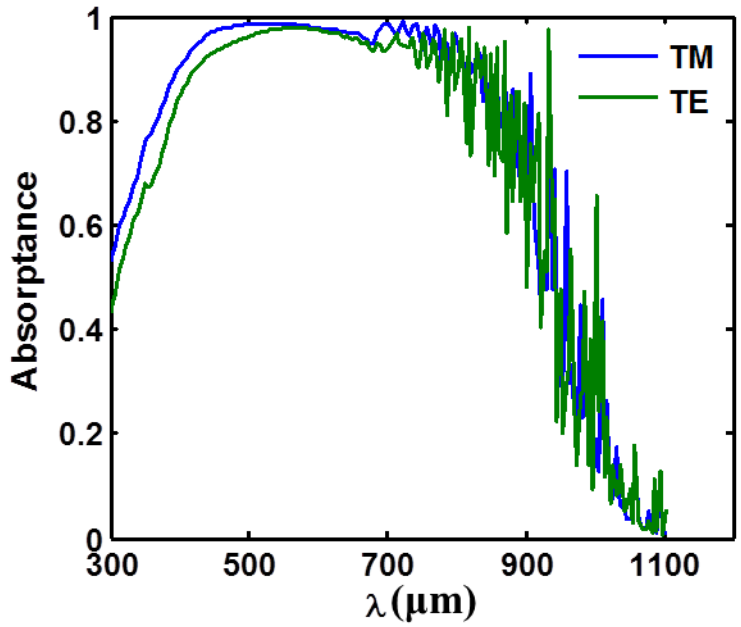

FIG. S4. Absorptances of TM and TE polarized light. A 100-nm-thick antireflective silicon nitride, 10-μm-thick c-Si, 200-nm-thick silicon dioxide, and 300-nm-thick silver are used, and the SG structure and normal incident light are assumed.

Section V. Profiles of Absorbed Intensity, Electric fields, and Magnetic Fields for Various Light-Trapping Cases

Profiles of absorbed intensity, electric fields, and magnetic fields are shown at wavelength of 1000nm for the front single grating (SG) case of W_{1s} = 700 nm , the matched double grating (DG) case of W_{1d} = 700 nm & W_{2d} = 700 nm, and the mismatched DG case of W_{1d} = 700 nm & W_{2d} = 3100 nm. Electric fields and magnetic fields in z direction are also indicating TE mode (E_z) and TM mode (H_z). These figures can show the interference pattern of diffractive modes from top and bottom gratings with diffractive angles, β_m, calculated from equation (2), and absorbed intensity profiles, Q_{rh}, in Fig. 3 can be seen as contribution from these two modes.

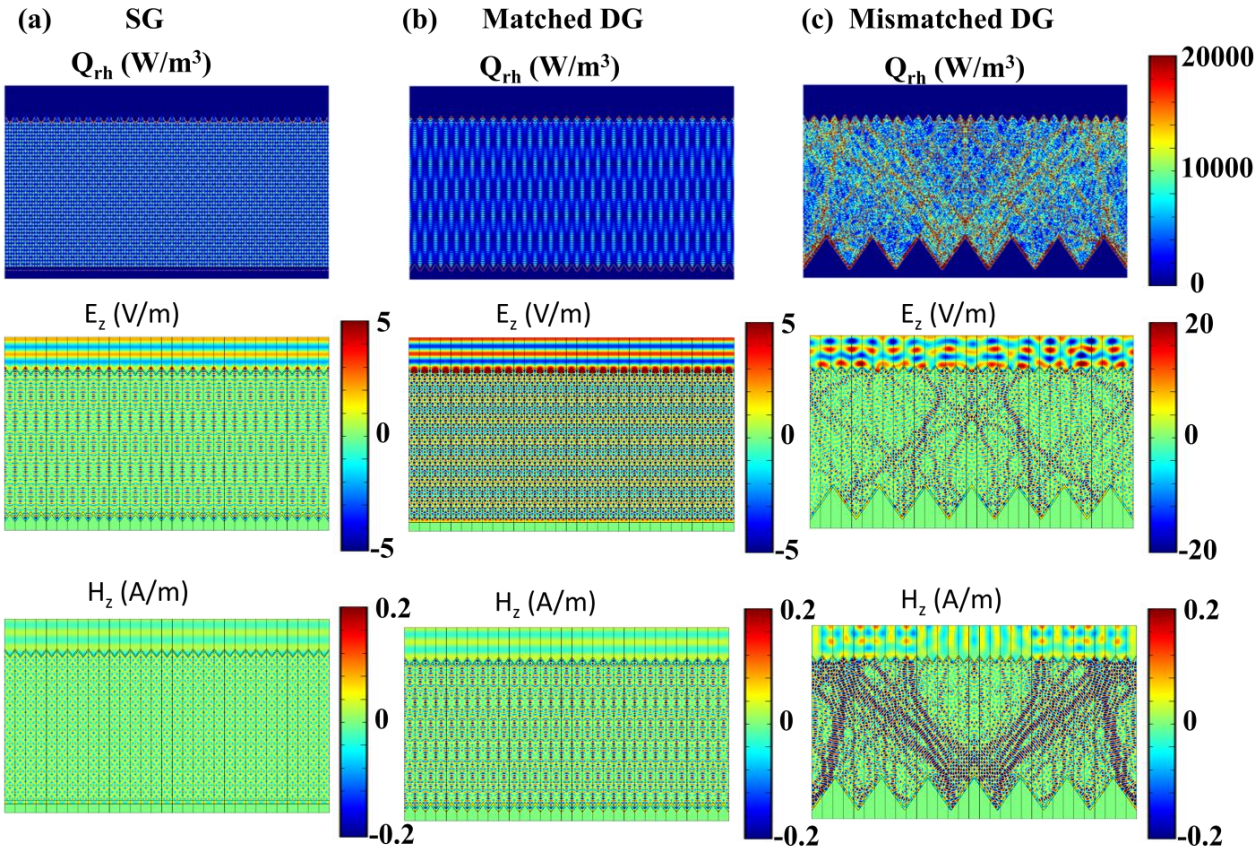

FIG. S5. The spatial distribution of the absorbed intensity, Qrh, in units of W/m^3 as calculated from numerical finite element simulations. Electric field in z direction (TE mode) in unit of V/m and magnetic field in z direction (TM mode) in unit of A/m at wavelength of 1000 nm and a spectral bandwidth of 4 nm. (a) The single grating (SG) case of W_{1s} = 700 nm. (b) The matched double grating (DG) case of W_{1d} = 700 nm & W_{2d} = 700 nm (c) The mismatched DG case of W_{1d} = 700 nm & W_{2d} = 3100 nm.

Section VI. Detail Combination of W_{1d} and W_{2d} in Fig. 4

Detail combination of top period, W_{1d}, and bottom period, W_{2d}, in Fig. 4 are listed in tables of this section. Table SI, SII, and SIII shows cases of W_{1d} = 700 nm, W_{1d} = 1300 nm, and W_{1d} = 2200 nm respectively. First row in each table indicates values of W_{1d}. Second, fifth, and eighth rows indicate values of W_{2d}, and third, sixth, and ninth rows show the corresponding values of least common multiple (LCM) of second, fifth, and eighth rows respectively. Fourth, seventh, and tenth rows show corresponding values of J_{ph} of second, fifth, and eighth rows respectively.

Table SI. Top and bottom period combinations of double gratings structure for **W_{1d} = 700 nm**

W_{1d} = 700 nm								
W_{2d} [nm]	**140**	**233.3**	**350**	**466.7**	**525**	**700**	**900**	**933.3**
W_{2d} / W_{1d}	$\frac{1}{5}$	$\frac{1}{3}$	$\frac{1}{2}$	$\frac{2}{3}$	$\frac{3}{4}$	1	$\frac{9}{7}$	$\frac{4}{3}$
LCM (W_{2d} ,W_{2d}) [nm]	700	700	700	1400	2100	700	6300	2800
J_{ph} [mA/cm^2]	33.7	33.49	33.58	34.64	35.12	33.33	36.38	35.57
W_{2d} [nm]	**1050**	**1166.7**	**1400**	**1750**	**2100**	**2200**	**2300**	**2450**
W_{2d} / W_{1d}	$\frac{3}{2}$	$\frac{5}{3}$	2	$\frac{5}{2}$	3	$\frac{22}{7}$	$\frac{23}{7}$	$\frac{7}{2}$
LCM (W_{2d} ,W_{2d}) [nm]	2100	3500	1400	3500	2100	15400	16100	2900
J_{ph} [mA/cm^2]	35.07	35.78	34.5	35.64	35.4	37.24	37.21	36
W_{2d} [nm]	**2800**	**3100**	**3500**	**3700**	**4200**	**4900**	**5600**	
W_{2d} / W_{1d}	4	$\frac{31}{7}$	5	$\frac{37}{7}$	6	7	8	
LCM (W_{2d} ,W_{2d}) [nm]	2800	21700	3500	25900	4200	4900	5600	
J_{ph} [mA/cm^2]	35.29	37.35	35.67	37.24	35.58	35.83	36.1	

Table SII. Top and bottom period combinations of double gratings structure for **W_{1d} = 1300[nm]**

W_{1d} = 1300 nm								
W_{2d} [nm]	**260**	**325**	**650**	**866.7**	**557.1**	**742.9**	**1733.3**	**928.6**
W_{2d} / W_{1d}	$\frac{1}{5}$	$\frac{1}{4}$	$\frac{1}{2}$	$\frac{2}{3}$	$\frac{3}{7}$	$\frac{4}{7}$	$\frac{4}{3}$	$\frac{5}{7}$
LCM (W_{2d} ,W_{2d}) [nm]	1300	1300	1300	2600	3900	5200	5200	6500
J_{ph} [mA/cm^2]	33.73	33.82	33.8	35.32	35.22	35.91	35.91	36.23
W_{2d} [nm]	**3033.3**	**1671.4**	**4766.7**	**2042.9**	**5633.3**	**2414.3**	**6933.3**	**2311.1**
W_{2d} / W_{1d}	$\frac{7}{3}$	$\frac{9}{7}$	$\frac{11}{3}$	$\frac{11}{7}$	$\frac{13}{3}$	$\frac{13}{7}$	$\frac{16}{3}$	$\frac{16}{9}$
LCM (W_{2d} ,W_{2d}) [nm]	9100	11700	14300	14300	16900	16900	20800	20800
J_{ph} [mA/cm^2]	36.67	37.18	36.94	37.27	36.9	37.41	36.86	37.68
W_{2d} [nm]	**2888.9**	**3714.3**	**1238.1**	**1300**	**2600**	**3900**	**5200**	
W_{2d} / W_{1d}	$\frac{20}{9}$	$\frac{20}{7}$	$\frac{20}{21}$	**1**	**2**	**3**	**4**	
LCM (W_{2d} ,W_{2d}) [nm]	26000	26000	26000	1300	2600	3900	5200	
J_{ph} [mA/cm^2]	37.88	37.94	37.85	34.11	35.34	35.67	35.7	

Table SIII. Top and bottom period combinations of double gratings structure for **W_{1d} = 2200[nm]**

W_{1d} = 2200 nm								
W_{2d} [nm]	**440**	**733.3**	**1100**	**1466.7**	**1650**	**2200**	**2933.3**	**3300**
W_{2d} / W_{1d}	$\frac{1}{5}$	$\frac{1}{3}$	$\frac{1}{2}$	$\frac{2}{3}$	$\frac{3}{4}$	1	$\frac{4}{3}$	$\frac{3}{2}$
LCM (W_{2d} ,W_{2d}) [nm]	2200	2200	2200	4400	6600	2200	8800	6600
J_{ph} [mA/cm^2]	34.46	34.42	34.33	35.46	36	34.47	36.29	35.94
W_{2d} [nm]	**3666.7**	**4400**	**5500**	**6600**	**1885.7**	**5133.3**	**1711.1**	**2514.3**
W_{2d} / W_{1d}	$\frac{5}{3}$	2	$\frac{5}{2}$	3	$\frac{6}{7}$	$\frac{7}{3}$	$\frac{7}{9}$	$\frac{8}{7}$
LCM (W_{2d} ,W_{2d}) [nm]	11000	4400	11000	6600	13200	15400	15400	17600
J_{ph} [mA/cm^2]	36.56	35.29	36.28	35.52	36.93	37.07	37.48	37.37
W_{2d} [nm]	**2828.6**	**3177.8**	**4085.7**					
W_{2d} / W_{1d}	$\frac{9}{7}$	$\frac{13}{9}$	$\frac{13}{7}$					
LCM (W_{2d} ,W_{2d}) [nm]	19800	28600	28600					
J_{ph} [mA/cm^2]	37.55	38.02	37.64					

Reference:

[1]*Elements of Photonics, Volume II : For Fiber and Integrated Optics;* Iizuka, K.; John Wiley & Sons, Inc.: New Jersey, 2002.

[2]H. Nagel, A. G. Aberle, and R. Hezel. *Prog. Photovolt: Res. Appl*. **7**, 245-260 (1999).

[3]H. H. Li, *J. Phys. Chem. Ref. Data*. **9**, 561-658 (1980).

[4]G. Vuye, S. Fisson, V. Nguyen Van, Y. Wang, J. Rivory, and F. Abeles, *Thin Solid Films* **233**, 166-170 (1993).

[5]I. H. Malitson, *J. Opt. Soc. Am.* **55**, 1205-1209 (1965).

[6]A. D. Rakic, A. B. Djurisic, J. M. Elazar, and M. L. Majewski, *Appl. Opt*. **37**, 5271-5283 (1998).

[7]D. E. Aspnes and A. A. Studna, *Phys. Rev. B* **27**, 985-1009 (1983).